Hole spin-flip transitions in a self-assembled quantum dot

Mateusz Krzykowski [ORCID],[*] Krzysztof Gawarecki [ORCID], and Paweł Machnikowski [ORCID]

Department of Theoretical Physics, Wrocław University of Science and Technology, Wybrzeże Wyspiańskiego 27, 50-370 Wrocław, Poland

In this work, we investigate hole spin-flip transitions in a single self-assembled InGaAs/GaAs quantum dot. We find the hole wave functions using the eight-band $\boldsymbol{k} \cdot \boldsymbol{p}$ model, and we calculate phonon-assisted spin relaxation rates for the ground-state Zeeman doublet. We systematically study the importance of various admixture and direct spin-phonon mechanisms giving rise to the transition rates. We show that the biaxial and shear strain constitute dominant spin-admixture coupling mechanisms. Then, we demonstrate that hole spin lifetime can be increased if a quantum dot is covered by a strain-reducing layer. Finally, we show that the spin relaxation can be described by an effective model.

I. INTRODUCTION

The dynamics of a carrier spin in semiconductor quantum dots (QDs), as well as other semiconductor nanostructures, is a subject of active study, both theoretical and experimental, due to potential implementations in the fields of spintronics and quantum information processing [1,2]. High-fidelity initialization [3,4], control [5,6], readout, and storage [7] of the information encoded in the spin are essential for future applications. These can be achieved with hole spin due to its relatively long coherence time [8], which is related to significantly weaker hyperfine interaction as compared to the electron case [9–11]. However, spin lifetimes and coherence times can be limited by the coupling to a phonon bath, leading to a loss of information to the environment [12–14].

The channels of phonon-induced spin-flip can be divided into two classes [13,15]. The first one contains various admixture mechanisms resulting from the spin-orbit coupling (SOC). Hence, a carrier state with some (dominant) spin orientation has also an admixture of the opposite spin. As a consequence, the coupling to a phonon bath can lead to spin-flip transitions between such states [12,13]. The second class of mechanisms results from direct spin-phonon coupling. In this case, the displacement field related to phonons lowers the symmetry, leading to spin relaxation in the presence of spin-orbit coupling [13,15–17].

The processes of hole spin-flip transition in a QD due to the mechanisms described above were widely studied [7,14,18–25]. It has been shown that phonon coupling via a piezoelectric field (PZ) is more important at small and moderate Zeeman splittings, while deformation potential (DP) coupling becomes dominate for larger splittings. In Ref. [25], the role of substrate orientation on hole spin relaxation was explored. It was shown that a self-assembled QD structure grown in the [111] direction offers up to one order of magnitude longer spin lifetimes compared to its [001]-oriented counterpart.

A detailed comparison of various spin relaxation channels was presented in Ref. [14]. Therein, the problem was studied within a four-band $\boldsymbol{k} \cdot \boldsymbol{p}$ model, neglecting structural strain, and combined with the approximation of parabolic potentials. It is known, however, that strain provides channels of spin mixing [26] that can significantly affect the spin relaxation [19]. In fact, recent results show a significant contribution from the structural shear strain to the s-p coupling between the hole states in a self-assembled InGaAs QD [25]. Since the s-p coupling is known as a major source of the opposite spin admixture [12,13], this suggest an important role of shear strain in phonon-assisted spin relaxation processes. Furthermore, biaxial strain opens also a spin-mixing channel [26–28], and its impact on the relaxation in self-assembled QDs has not been studied so far.

The spin-orbit interaction, combined with inversion symmetry breaking, creates a number of coupling mechanisms [26,28,29] that need to be taken into account when simulating spin relaxation processes. To associate these processes with symmetry-lowering strain fields appearing on the mesoscopic level, we propose a description in the framework of the multiband $\boldsymbol{k} \cdot \boldsymbol{p}$ model. In this approach, the physical processes are accounted for by individual terms in the Hamiltonian that follow from a rigorous symmetry-based analysis in terms of invariants [28], and they are often related to effective spin-orbit terms that have appeared in the literature over many decades [15] (although mostly for electrons, rather than holes). In this way, the $\boldsymbol{k} \cdot \boldsymbol{p}$ method provides an alternative and complementary view of the nanostructure properties as compared to the very exact but more computationally intensive atomistic methods [30–33], while retaining a sufficient accuracy. This approach not only allows one to identify the relevant symmetry-related relaxation channels that might be mitigated by QD structure engineering, but it also offers a physical picture based on symmetry, in line with the general development of condensed-matter physics [34]. Here, we gain physical insight into the properties of interest, and we compare the relevance of individual coupling mechanisms by selectively "turning on/off" the corresponding terms in the

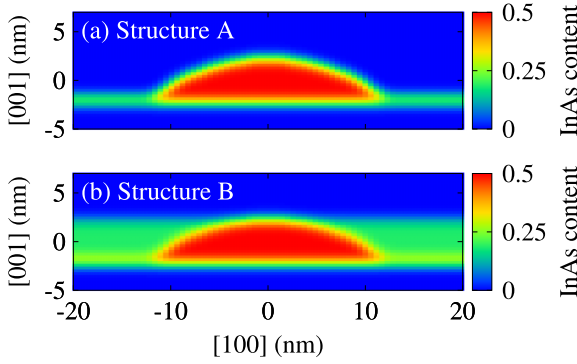_____

[*]Mateusz.Krzykowski@pwr.edu.pl

FIG. 1. In$_x$Ga$_{1-x}$As distribution in the system for the single QD (a) and the QD capped by the SRL (b).

$\boldsymbol{k} \cdot \boldsymbol{p}$ Hamiltonian. Furthermore, the eight-band $\boldsymbol{k} \cdot \boldsymbol{p}$ method offers a well-established way to incorporate the carrier-phonon interaction, which is based on the Bir-Pikus Hamiltonian, expressed in terms of the phonon modes [15,18,35].

In this paper, we systematically study the importance of various phonon-induced spin-flip transition mechanisms for a hole confined in an InGaAs/GaAs quantum dot system. The hole states are calculated using the full eight-band $\boldsymbol{k} \cdot \boldsymbol{p}$ method for a realistic geometry of the system. The structural strain distribution is accounted for within the continuous elasticity approach. The hole is subject to an external magnetic field applied parallel to the growth direction as well as coupled to an acoustic phonon reservoir via deformation potential and piezoelectric field. We show that the effect of spin-admixture mechanisms (dominant at low and moderate magnetic fields) coming from the shear and biaxial strain can be limited by the presence of a strain-reducing layer. Finally, we show that transitions via the spin-admixture channels can be accounted for using an effective model with Gaussian-like heavy-hole wave functions.

The paper is organized as follows. In Sec. II, we describe the QD geometry and discuss the model used in the calculations. In Sec. III, we present the results for various spin-flip transition mechanisms, and we introduce an effective model describing the relaxation due to spin-admixture effects. We conclude the article in Sec. IV.

II. MODEL

We consider a single, self-assembled QD of In$_{0.5}$Ga$_{0.5}$As/GaAs [structure A, Fig. 1(a)]. The material intermixing is simulated by a Gaussian blur of the composition with the standard deviation of 0.6 nm. We model the dot as a lens-shaped structure with a base radius of 21a, a height of 7a, and a wetting layer of thickness a, where a is the GaAs lattice constant. In the case of structure B [see Fig. 1(b)], the QD is capped by an In$_{0.188}$Ga$_{0.812}$As/GaAs strain-reducing layer (SRL) of constant thickness. The In content in the SRL was chosen so that g-factors in both structures are equal up to <1%. Such layers are often utilized to tune QD emission to a desired range [36–38]. In this paper, we use a SRL to soften strain at the interfaces.

The strain field caused by the lattice mismatch of InAs and GaAs materials is calculated using the continuous

elasticity approach [39]. The piezoelectric potential (inevitable in zinc-blende structure in the presence of shear strain) is calculated including polarization up to second order in strain tensor elements [40], where we use parameters from Ref. [41]. Hole wave functions are obtained using the eight-band $\boldsymbol{k} \cdot \boldsymbol{p}$ model [28,42]. We incorporated magnetic field according to the gauge-invariant scheme described in Ref. [43]. The computational domain is discretized on a Cartesian mesh of $a \times a \times (a/2)$ cell size. The $\boldsymbol{k} \cdot \boldsymbol{p}$ model and its implementation are described in detail in the Appendix of Ref. [44] [where we took the parameter κ' expressed in terms of the modified Luttinger parameters, i.e., $\kappa' = -\frac{1}{3}(\gamma_1' - 2\gamma_2' - 3\gamma_3' + 3)$].

The inversion symmetry breaking on the level of the zinc-blende lattice structure gives rise to many spin-orbit couplings between the bands. These effects are inherently accounted for by the extended (14-band) Kane $\boldsymbol{k} \cdot \boldsymbol{p}$ Hamiltonian [28,45,46]. Such a model contains the valence bands (Γ_{8v} and Γ_{7v} band blocks) built by the p-type bonding orbitals, and the conduction bands (Γ_{6c}, Γ_{7c}, and Γ_{8c}) composed of the s- and p-type antibonding orbitals. The reduction of this model to the two-band $\boldsymbol{k} \cdot \boldsymbol{p}$ via Löwdin elimination leads to an appearance of the $\propto k^3$ terms (known as the Dresselhaus term) [28]. In the framework of the eight-band $\boldsymbol{k} \cdot \boldsymbol{p}$, the Dresselhaus coupling enters the Hamiltonian via the perturbative $\propto k^2$ terms [28],

$$
H_{6c8v}^{(D)} = i\sqrt{3}B_{8v}^+[T_x\{k_y, k_z\} + \text{c.p.}]
$$
$$
+ \frac{\sqrt{3}}{6}B_{8v}^-(T_{xx} - T_{yy})(2k_z^2 - k_x^2 - k_y^2)
$$
$$
- \frac{\sqrt{3}}{2}B_{8v}^- T_{zz}(k_x^2 - k_y^2),
$$
$$
H_{6c7v}^{(D)} = -\frac{i}{\sqrt{3}}B_{7v}[\sigma_x\{k_y, k_z\} + \text{c.p.}],
$$

where $\{A, B\} = \frac{1}{2}(AB + BA)$, σ_n are the Pauli matrices, T_n are matrices connecting the $j = 1/2$ and $3/2$ representations, J_n are matrices of the $j = 3/2$ representation of angular momentum, $T_{nm} = T_n J_m + T_m J_n$ (with the explicit forms of the matrices provided in [47]), and c.p. denotes cyclic permutations. The Kane off-diagonal parameters are given by [28]

$$
B_{8v}^+ = -\frac{i}{2}P'Q\left(\frac{1}{E_g - E_g' - \Delta'} - \frac{1}{E_g' + \Delta'} \right.
$$
$$
\left. + \frac{1}{E_g - E_g'} - \frac{1}{E_g'}\right),
$$
$$
B_{8v}^- = -\frac{i}{2}P'Q\left(\frac{1}{E_g' + \Delta'} - \frac{1}{E_g - E_g' - \Delta'} \right.
$$
$$
\left. + \frac{1}{E_g - E_g'} - \frac{1}{E_g'}\right),
$$
$$
B_{7v} = -iP'Q\left(\frac{1}{E_g - E_g' - \Delta'} - \frac{1}{E_g' + \Delta + \Delta'}\right),
$$

where P' and Q are parameters proportional to the interband momentum matrix elements, E_g (E_g') is the energy gap

between the 6c and 8v (7c and 8v) bands, and Δ (Δ') is the spin-orbit splitting between the 8v and 7v (8c and 7c) bands.

In Ref. [48], it has been shown that also the off-diagonal spin-orbit parameter Δ^- contributes significantly to the Dresselhaus coupling. Such a parameter is related to a different ionicity of anions and cations in a crystal and couples the 8c and 7c band blocks in the 14-band $\boldsymbol{k} \cdot \boldsymbol{p}$ model [48,49]. To represent its influence in the eight-band $\boldsymbol{k} \cdot \boldsymbol{p}$ Hamiltonian, we performed calculations within the Löwdin perturbation theory, which gives the off-diagonal terms

$$H_{6c8v}^{(\Delta^-)} = \frac{\sqrt{3}}{2} D_1 (T_x k_x + \text{c.p.}),$$

$$H_{6c7v}^{(\Delta^-)} = -\frac{1}{\sqrt{3}} D_2 (\sigma_x k_x + \text{c.p.}),$$

where

$$D_1 = -\frac{1}{3} P'^* \Delta^- \left(\frac{1}{E_g - E'_g - \Delta'} - \frac{1}{E'_g + \Delta'} \right),$$

$$D_2 = \frac{1}{3} P'^* \Delta^- \left(\frac{1}{E_g - E'_g} - \frac{1}{E'_g + \Delta} \right),$$

where $\Delta^-[\text{InAs}] = -0.05$ eV and $\Delta^-[\text{GaAs}] = -0.17$ eV [48], while the other parameters are given in Refs. [28,44]. Finally, the bulk inversion asymmetry enters via the k-linear terms in the Hamiltonian [28,42],

$$H_{8v8v}^{(\text{k})} = \frac{2}{\sqrt{3}} C_{\text{k}} (\{J_x, J_y^2 - J_z^2\} k_x + \text{c.p.}),$$

$$H_{8v7v}^{(\text{k})} = -i\sqrt{3} C_{\text{k}} (T_{yz}^\dagger k_x + \text{c.p.}),$$

where $C_{\text{k}}[\text{InAs}] = -0.0034$ eVÅ and $C_{\text{k}}[\text{GaAs}] = -0.0112$ eVÅ [28].

In addition to the inevitable inversion symmetry breaking due to the zinc-blende crystal lattice, the symmetry of the system can be further reduced by the presence of strain. It is known that uniaxial stress (for some crystal directions) leads to a strain-dependent $\boldsymbol{k}$-linear splitting in the conduction band [27,50,51]. In the eight-band $\boldsymbol{k} \cdot \boldsymbol{p}$ model, this effect enters the Hamiltonian via the off-diagonal terms [26],

$$H_{\text{str},6c8v} = i\sqrt{3} C_2 [T_x \epsilon_{yz} + \text{c.p.}],$$

$$H_{\text{str},6c7v} = -i\frac{1}{\sqrt{3}} C_2 [\sigma_x \epsilon_{yz} + \text{c.p.}],$$

where ϵ_{ij} are strain tensor components. Due to the lack of available experimental data for InAs, we assume the value of parameter C_2 for In$_x$Ga$_{1-x}$As as $C_2(x) = 0.4 E_g(x)[E_g(x) + \Delta(x)]/\Delta(x)$, where 0.4 was extracted from the experimental data for GaAs [52].

The symmetry reduction caused by the uniaxial stress leads to spin-orbital effects in the valence band as well [27,53]. Such a strain-induced $\boldsymbol{k}$-linear splitting is represented by the terms [26,28]

$$H_{\text{str},8v8v}^{(\text{k})} = [C_4(\epsilon_{yy} - \epsilon_{zz})k_x]J_x + \text{c.p.},$$

$$H_{\text{str},8v7v}^{(\text{k})} = \frac{3}{2}[C_4(\epsilon_{yy} - \epsilon_{zz})k_x]T_x^\dagger + \text{c.p.},$$

$$H_{\text{str},7v7v}^{(\text{k})} = [C_4(\epsilon_{yy} - \epsilon_{zz})k_x]\sigma_x + \text{c.p.},$$

where the form of $H_{\text{str},7v7v}^{(\text{k})}$ was derived from the table of irreducible tensor components of the T_d point group given in Ref. [28]. There are significant discrepancies in the reported values of the C_4 parameter. While the empirical pseudopotential method (EPM) gives $C_4[\text{InAs}] = 2.9$ eVÅ and $C_4[\text{GaAs}] = 3.2$ eVÅ, the results of the sp^3 tight-binding (TB) model suggest $C_4[\text{InAs}] = 7.0$ eVÅ and $C_4[\text{GaAs}] = 6.8$ eVÅ [54]. In the present paper, we utilize the latter values.

The full Hamiltonian of the system can be written as [55]

$$H = \sum_n E_n h_n^\dagger h_n + \sum_{\lambda, \boldsymbol{q}} \hbar\omega_{\lambda, \boldsymbol{q}} b_{\lambda, \boldsymbol{q}}^\dagger b_{\lambda, \boldsymbol{q}} + \sum_{ij} V_{ij} h_i^\dagger h_j,$$

where E_n describes the energy of the nth state, and $h_n^{(\dagger)}$ is the related annihilation (creation) operator. The second term accounts for the phonon bath, where $\lambda \in \{l, t_1, t_2\}$ denotes the acoustic phonon branch (a single longitudinal and two transversal modes, respectively), $\boldsymbol{q}$ is a wave vector, $\hbar\omega_{\lambda, \boldsymbol{q}}$ is a phonon mode energy, and $b_{\lambda, \boldsymbol{q}}^{(\dagger)}$ is the annihilation (creation) operator of the mode. We assume the linear dispersion $\omega_{\lambda, \boldsymbol{q}} = c_\lambda q$ with a branch-dependent speed of sound $c_l = 5150$ m/s and $c_{t1/t2} = 2800$ m/s [56]. The last term accounts for the hole-phonon interaction

$$V_{ij} = \int d^3 \boldsymbol{r} \, \Psi_i^\dagger(\boldsymbol{r}) [H_{\text{DP}}^{(\text{ph})}(\boldsymbol{r}) + V_{\text{PZ}}^{(\text{ph})}(\boldsymbol{r})] \Psi_j(\boldsymbol{r}),$$

where $\Psi_i(\boldsymbol{r})$ is a wave function of the ith hole state in the form of eight-component pseudospinors [28,57], while $H_{\text{DP}}^{(\text{ph})}$ and $V_{\text{PZ}}^{(\text{ph})}$ represent the carrier-phonon couplings via deformation potential and piezoelectric field, respectively.

The deformation potential coupling is described by the Bir-Pikus Hamiltonian supplemented with the C_2-strain terms [26,28,42],

$$
\begin{aligned}
H_{\text{DP}}^{(\text{ph})}(\boldsymbol{r}) = -\Bigg\{ & a_\text{c} \text{Tr} \hat{\epsilon}(\boldsymbol{r}) \mathbb{I}^{(6c)} + a_\text{v} \text{Tr}\{\hat{\epsilon}(\boldsymbol{r})\} \mathbb{I}^{(8v+7v)} \\
& - b_\text{v}\left[\left(J_x^{(8v)2} - \frac{1}{3} J^{(8v)2}\right) \epsilon_{xx}(\boldsymbol{r}) + \text{c.p.} \right] \\
& - \frac{d_\text{v}}{\sqrt{3}} [2\{J_x^{(8v)}, J_y^{(8v)}\} \epsilon_{xy}(\boldsymbol{r}) + \text{c.p.}] \\
& - 3b_\text{v} [(T_{xx}^{(7v8v)} + \text{H.c.}) \epsilon_{xx}(\boldsymbol{r}) + \text{c.p.}] \\
& - 2\sqrt{3} d_\text{v} [(T_{xy}^{(7v8v)} + \text{H.c.}) \epsilon_{xy}(\boldsymbol{r}) + \text{c.p.}] \\
& + \sqrt{3} C_2 [(iT_x^{(6c8v)} + \text{H.c.}) \epsilon_{yz}(\boldsymbol{r}) + \text{c.p.}] \\
& - \frac{1}{\sqrt{3}} C_2 [(i\sigma_x^{(6c7v)} + \text{H.c.}) \epsilon_{yz}(\boldsymbol{r}) + \text{c.p.}] \Bigg\},
\end{aligned}
$$

where the global "$-$" sign results from the description in the hole picture; a_c, a_v, b_v, and d_v are deformation potentials; $\hat{\epsilon}(\boldsymbol{r})$ is the (phonon-induced) strain-tensor field; $\mathbb{I}$ is an identity matrix; and σ, J, T are matrices used for the invariant expansion of the Hamiltonian, with the superscripts referring to the band blocks [47]. We take GaAs values for all deformation potentials and the C_2 parameter. To obtain $H_{\text{DP}}^{(\text{ph})}$ in the representation of phonon normal modes, we perform the

expansion

$$\epsilon_{ij}(\boldsymbol{r}) = \sum_{\lambda,\boldsymbol{q}} \epsilon_{ij}^{(q,\lambda)} e^{i\boldsymbol{q}\cdot\boldsymbol{r}},$$

with the coefficients [55]

$$\epsilon_{ij}^{(q,\lambda)} = -\frac{1}{2}\sqrt{\frac{\hbar}{2V\rho\omega_{\lambda,\boldsymbol{q}}}}(\hat{e}_{q\lambda,i}q_j + \hat{e}_{q\lambda,j}q_i)(b_{-\boldsymbol{q},\lambda}^{\dagger} + b_{\boldsymbol{q},\lambda}),$$

where $\rho = 5350$ kg/m^3 [56] and V denote the density and the volume in the bulk crystal, respectively, and $\hat{e}_{q\lambda,i}$ is the ith component of the polarization unit vector.

The coupling via piezoelectric field potential is given by $V_{\text{PZ}}^{(\text{ph})} = e\phi(\boldsymbol{r})\mathbb{I}^{(6c+8v+7v)}$, where e is the elementary charge, $\phi(\boldsymbol{r})$ is the phonon-induced electrostatic potential given by [55,58]

$$\phi(\boldsymbol{r}) = i\frac{2d_{14}}{\varepsilon_0\varepsilon_r}\sum_{\boldsymbol{q},\lambda}\frac{1}{q^2}\left(q_x\epsilon_{yz}^{(q,\lambda)} + \text{c.p.}\right)e^{i\boldsymbol{q}\cdot\boldsymbol{r}},$$

where $\varepsilon_r = 12.4$ is the relative dielectric constant (here assumed equal to the bulk GaAs value [59]), and $d_{14} = -0.16$ C/m^2 is the element of the piezoelectric tensor (in a zinc-blende crystal only one component is linearly independent) for GaAs [60].

The interaction Hamiltonian can be expressed by

$$V_{\text{int}} = \sum_{\lambda,\boldsymbol{q}} \mathcal{V}(\boldsymbol{q},\lambda)e^{i\boldsymbol{q}\cdot\boldsymbol{r}},$$

where $\mathcal{V}(\boldsymbol{q},\lambda)$ contains $H_{\text{DP}}^{(\text{ph})}$ and $V_{\text{PZ}}^{(\text{ph})}$ for a single-phonon mode $(\boldsymbol{q},\lambda)$. We calculate the phonon-induced relaxation rates using the Fermi golden rule. The rate between the i and j states is $\Gamma_{ij} = 2\pi R_{ijji}(\omega_{ij})$, where $\omega_{ij} = (E_i - E_j)/\hbar$, and $R_{ijji}(\omega)$ is the phonon spectral-density given by [55]

$$R_{ijji}(\omega) = \frac{1}{\hbar^2}\sum_{\lambda,\boldsymbol{q}}|\langle\psi_i|\mathcal{V}(\boldsymbol{q},\lambda)e^{i\boldsymbol{q}\cdot\boldsymbol{r}}|\psi_j\rangle|^2\delta(\omega - \omega_{\lambda,\boldsymbol{q}}),$$

where we assume absolute zero temperature.

III. RESULTS

A. Full model

In this section, we analyze hole spin-flip transitions due to two distinct classes of mechanisms. The first class is induced by band-off-diagonal terms in the multiband carrier-phonon interaction Hamiltonian. As discussed in detail in Ref. [15], when the multiband Hamiltonian is reduced to an effective two-band model (describing the two heavy-hole subbands in the present case) via Löwdin perturbational decoupling, such terms lead to direct spin-phonon couplings in the effective Hamiltonian. The second mechanism relies on the band-off-diagonal terms unrelated to phonons that express various spin-orbit couplings. As a result, the predominantly heavy-hole state with a certain nominal spin orientation has contributions (admixtures) of states with the opposite spin. Therefore, states with nominally opposite spins may be coupled via spin-conserving phonon terms (stemming from the diagonal elements in the $\boldsymbol{k}\cdot\boldsymbol{p}$ representation). Although Löwdin elimination is of less practical use for holes than for
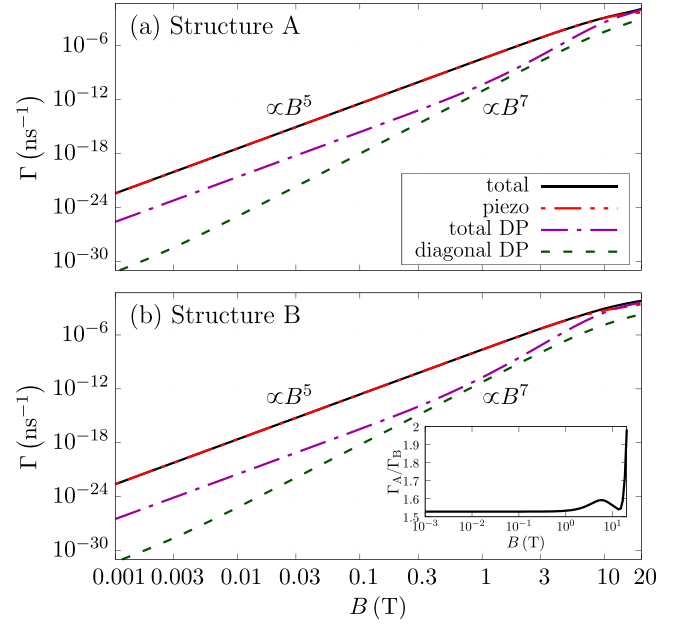

FIG. 2. Phonon-induced spin-flip relaxation rate in the lowest-energy Zeeman doublet as a function of axial magnetic field for the QD structures A and B. Solid black line indicates total rate, while dashed colored lines indicate various contributions. The lines are ordered depending on their contribution to the considered process from greatest to lowest at low magnetic fields. The inset in panel (b) presents the ratio between total relaxation rates in the considered structures.

electrons, the relation between the location of the phonon term in the $\boldsymbol{k}\cdot\boldsymbol{p}$ Hamiltonian and the form of the resulting effective term still holds in principle and allows one to classify the numerous spin relaxation channels. Therefore, we will use the terms *spin-phonon* and *admixture* to label spin-flip mechanisms in the following discussion, even though we study the full multiband $\boldsymbol{k}\cdot\boldsymbol{p}$ model.

In Fig. 2, we present spin-flip relaxation rates due to the interaction with the acoustic phonon reservoir as a function of the magnetic field B applied parallel to the growth axis [001]. Various lines in the figure correspond to particular contributions to the interaction Hamiltonian. The rates are given for the two QD structures (see Fig. 1) differing by the presence or absence of the SRL and therefore strain distribution in the system. For low-to-moderate magnetic fields, the coupling via piezoelectric field dominates, however above 10 T for the structures this effect starts to saturate and the coupling via the deformation potential becomes dominant. This effect is caused by different power dependencies of various spin-flip channels on magnetic field [14,15]. The coupling via a phonon-induced piezoelectric field exhibits $\propto B^5$ behavior. On the other hand, the coupling via a deformation potential contains terms that increase like $\propto B^5$, $\propto B^7$, and even $\propto B^9$, which is clearly visible in the line slopes in the logarithmic scale. The $\propto B^9$ contribution is related to some of the d_v shear-strain off-diagonal terms in $H_{\text{DP}}^{(\text{ph})}$. Since in our approach $V_{\text{PZ}}^{(\text{ph})}$ is diagonal, it is spin-conserving and gives rise to the spin-flip relaxation due to the admixture mechanisms only. On the other hand, for the coupling via the deformation potential, the
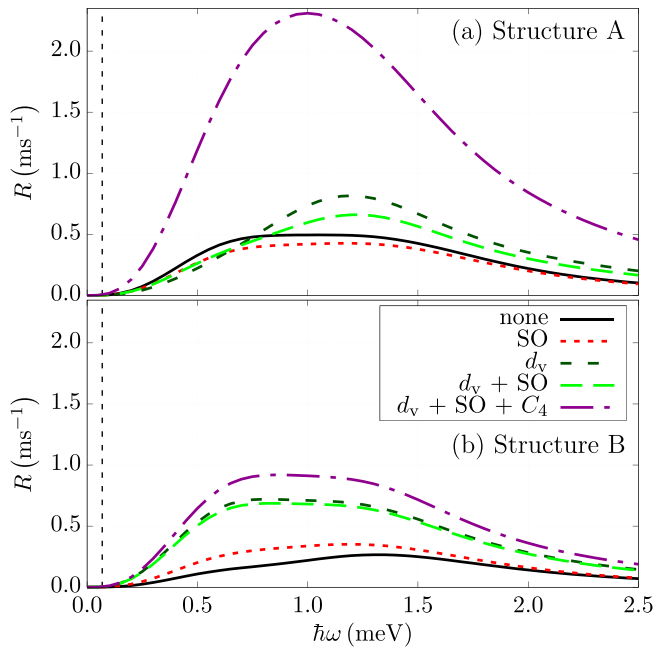
FIG. 3. Phonon spectral density at $B = 1$ T for the QD structures A and B, representing the absence and presence of a SRL, respectively. The solid black line represents the background related to various contributions, with all explicit Hamiltonian terms being turned off. Colored dashed lines represent cases of explicit terms being taken into account. The vertical line corresponds to the energy difference $E_2 - E_1$ between the states in a Zeeman doublet.

off-diagonal terms clearly dominate over the diagonal part. As a consequence, for high magnetic fields the direct spin-phonon coupling is the most significant class of mechanisms.

We have compared the relaxation rates for the structures with and without the SRL [see the inset in Fig. 2(b)]. In the presence of the SRL, the relaxation due to strain-related spin admixtures slows down. As a consequence, the SRL increases the spin lifetime for weak and moderate magnetic fields, where the admixture mechanisms dominate, in this case by about 50%. On the other hand, in structure B the direct spin-phonon mechanism is also weaker. This leads to up to a twofold increase of spin lifetime in the high magnetic field regime.

We have investigated the importance of various spin admixture mechanisms to the phonon-assisted spin-flip relaxation rate. This could be done by artificially turning on and off relevant explicit terms in the eight-band $\boldsymbol{k} \cdot \boldsymbol{p}$ Hamiltonian. However, this may strongly affect the hole g-factor, hence the resulting relaxation rates correspond to different energies, making them hard to compare. Instead, we studied the relevant spectral densities (Fig. 3). To remove all of the contributions coming from the direct spin-phonon mechanisms, we took into consideration only the coupling via the piezoelectric field. We performed the simulations for both considered QD systems at $B = 1$ T (where, according to Fig. 2, the coupling via the PZ field is the dominant contribution).

In the case of the QD without the SRL [Fig. 3(a)], the dominant contribution is the biaxial strain (terms proportional to C_4). Other significant contributions come from the shear

strain in the valence band (terms proportional to d_v in the Bir-Pikus Hamiltonian) as well as the background related to the remaining contributions, such as the Rashba effect coming from structure inversion asymmetry (SIA), represented in Fig. 3 as a solid black line. These results are consistent with Ref. [25], where d_v shear-strain terms were shown as one of the most important contributions determining the hole s-p coupling. The contribution from the Dresselhaus bulk inversion asymmetry (BIA) spin-orbit coupling is relatively small for structure A, and it interferes destructively with the background.

In the case of structure B [where SRL is included, Fig. 3(b)], the dominant C_4 contribution is significantly quenched, leading to an almost threefold reduction in spectral density. The Dresselhaus term remains mostly unchanged while the background contributions are reduced. This is to be expected for a low-strain regime, where the Dresselhaus effect can be the dominant spin-admixture-related relaxation channel [14]. In contrast to the electron case [15], for both considered structures the effect of off-diagonal terms linear in momentum and strain (in H_{6c8v} and H_{6c7v} blocks) is negligible. Furthermore, the influence of C_2-strain is small and is included in the background for clarity.

The exact values obtained in our calculations depend, to some extent, on the assumed values of the parameters and on the choice of the theoretical approach. For instance, atomistic calculations, commonly considered to be the most accurate method available for QD structures, might yield slightly different values. It has been shown, however, that the agreement between the $\boldsymbol{k} \cdot \boldsymbol{p}$ and tight-binding methods is good upon appropriate extension of the strain terms in the former [61]. To check the robustness of our conclusions, we have repeated our calculations using a model from Ref. [61] with nonlinear corrections to the strain terms that yield good quantitative agreement with the tight-binding approach. We have found that the change in the spectral densities is almost unnoticeable, and the relaxation rates do not change considerably when comparing structures with the same Zeeman splitting. The major effect of the nonlinear corrections is a modification of the g-factor by several percent, which corresponds trivially to a noticeable increase of the spin-flip rate via a strong dependence of the phonon-assisted relaxation on the Zeeman splitting. Therefore, there are no reasons to expect that another choice of parametrization or even switching to an atomistic method would affect our main qualitative conclusion on the predominant role of strain-induced symmetry lowering in generating spin-relaxation channels in a self-assembled structure.

B. Effective model

The hole phonon-assisted spin-flip relaxation rates can be accounted for using wave functions obtained from the effective model with empirical parameters fitted to the $\boldsymbol{k} \cdot \boldsymbol{p}$ simulation data (see Table I). We use heavy-hole Gaussian wave functions and a simple hole Hamiltonian based on the Fock-Darwin model, supplemented by additional terms accounting for the spin-orbit interaction [25].

Let us consider the basis of s- and p-type states $\{|0\Uparrow\rangle, |0\Downarrow\rangle, |+1\Uparrow\rangle, |+1\Downarrow\rangle, |-1\Uparrow\rangle, |-1\Downarrow\rangle\}$, where the indices correspond to the axial projections of envelope and

TABLE I. Effective Hamiltonian and Gaussian wave-function parameters used in the effective model calculations.

$\Delta V_0^{(p)}$	16.04 meV	$V_{pp}^{(so)}$	6.063 meV
V_a	2.849 meV	$V_{sp}^{(so)}$	165.2 μeV
g_s	1.182	α_s	2.212 μeV/T^2
g_p	4.596	α_p	4.572 μeV/T^2
W	-0.335 meV/T		
l_z	15.69 nm	l_p	55.79 nm

band angular momentum ($j_z = \pm 3/2$), respectively. The wave functions used for the calculations are Gaussians expressed in a cylindrical coordinate system,

$$\psi_0^{(v)}(r,z) = \frac{1}{\sqrt{\pi^{\frac{3}{2}} l_p^2 l_z}} \exp\left(-\frac{r^2}{2l_p^2} - \frac{z^2}{2l_z^2}\right)\chi_v,$$

$$\psi_{\pm 1}^{(v)}(r,\phi,z) = \frac{r}{\sqrt{\pi^{\frac{3}{2}} l_p^4 l_z}} \exp\left(-\frac{r^2}{2l_p^2} - \frac{z^2}{2l_z^2}\right)\exp(\pm i\phi)\chi_v,$$

where χ_v is a spinor corresponding to the axial projection of the band angular momentum, and l_p and l_z describe the spatial extension of the wave function in the xy plane and along the z axis, respectively. The effective Hamiltonian written in the considered basis is given by [25]

$$
\begin{aligned}
H_{\text{eff}} = {}& \Delta V_0^{(p)}(|1\rangle\langle 1| + |-1\rangle\langle -1|) \otimes \mathbb{I}_2 \\
& + \tfrac{1}{2}eV_{pp}^{(so)}L_z \otimes \sigma_z + WB_z L_z \otimes \mathbb{I}_2 + \tfrac{1}{2}\mu_B[g_s|0\rangle\langle 0| \\
& + g_p(|1\rangle\langle 1| + |-1\rangle\langle -1|)]B_z \otimes \sigma_z \\
& + V_a(|1\rangle\langle -1| + |-1\rangle\langle 1|) \otimes \mathbb{I}_2 \\
& + V_{sp}^{(so)}[(|0\rangle\langle -1| \otimes |\Uparrow\rangle\langle\Downarrow| \\
& - |0\rangle\langle 1| \otimes |\Downarrow\rangle\langle\Uparrow|) + \text{H.c.}] \\
& + [\alpha_s|0\rangle\langle 0| + \alpha_p(|1\rangle\langle 1| + |-1\rangle\langle -1|)]B_z^2 \otimes \mathbb{I}_2,
\end{aligned}
$$

where $\Delta V_0^{(p)}$ is a bare energy difference between s- and p-type states at $B=0$, V_a is a parameter related to the anisotropy, W is a parameter accounting for the influence of the envelope angular momentum, μ_B is the Bohr magneton, $g_{s/p}$ are effective g-factors for s- and p-type states, respectively, $V_{pp}^{(so)}$ corresponds to the spin-orbit coupling for the p-type states, $V_{sp}^{(so)}$ describes coupling between s- and p-type states involving change in both envelope and band angular momenta, $\alpha_{s/p}$ are diamagnetic parameters for s/p-type orbitals, L_z is the operator of the axial component of the envelope angular momentum, σ_z is the axial Pauli matrix, and finally $\mathbb{I}_n$ is an identity matrix of order n. All of the parameters describing the effective Hamiltonian are fitted to the magnetic-field dependence of the energy levels obtained from the eight-band $\boldsymbol{k}\cdot\boldsymbol{p}$ (see details in Refs. [25,44]). The numerical values of the parameters are compiled in the Table I. Since the fitting procedure gives only the absolute values of parameters, the relative phases of terms in H_{eff} are assumed. We also neglected terms $|0\rangle\langle -1| \otimes |\Downarrow\rangle\langle\Uparrow| + \text{H.c.}$ and $|0\rangle\langle 1| \otimes |\Uparrow\rangle\langle\Downarrow| + \text{H.c.}$ since they are not represented by any avoided crossing in target magnetic-field energy dependence [25]. The param-
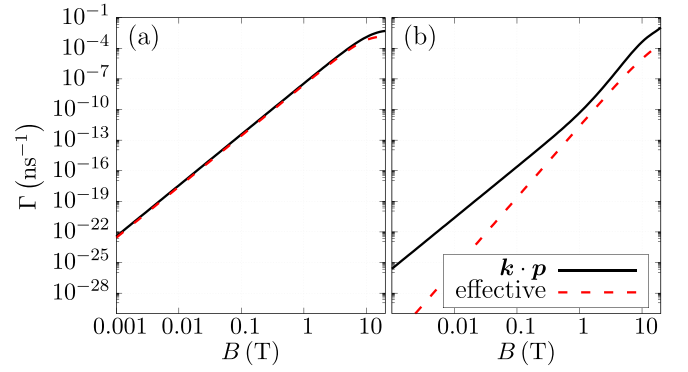

FIG. 4. Phonon-induced spin-flip relaxation rate via piezoelectric effect (a) and deformation potential (b) couplings as a function of magnetic field B for realistic $\boldsymbol{k}\cdot\boldsymbol{p}$ calculations (solid black) and the effective model (dashed red).

eters describing the wave-function spatial extension (l_p, l_z) are extracted from probability density maps at $B=0$. Finally, the effective Hamiltonian 6×6 matrix is diagonalized, and relaxation rates are calculated using the Fermi golden rule (with the same interaction Hamiltonian as in the full model).

We compare the values of relaxation rates obtained from the effective model and eight-band $\boldsymbol{k}\cdot\boldsymbol{p}$ calculations for the QD without SRL (structure A). Figure 4(a) presents the spin-flip relaxation rate via piezoelectric field alone. The results show a reasonable agreement, and the characteristic $\propto B^5$ dependence. In Fig. 4(b) we present a similar comparison, but for the coupling via the deformation potential alone. In this case, the results strongly disagree. In particular, the effective model does not reproduce the $\propto B^5$ and $\propto B^9$ dependence regimes characteristic for direct spin-phonon coupling.

IV. CONCLUSIONS

We have presented a theoretical study of the hole phonon-assisted spin-flip relaxation in a self-assembled QD systems. With wave functions found using the eight-band $\boldsymbol{k}\cdot\boldsymbol{p}$ method, we have calculated relaxation rates related to the phonon coupling via the deformation potential and the piezoelectric field. In this framework, we have investigated the contributions coming from various channels belonging to the spin-admixture and direct spin-phonon classes of mechanisms. We have shown that the dominating spin-admixture terms come from the biaxial and shear strain. We have shown that (for low and moderate magnetic fields) the QD covered by a strain-reducing layer offers a significantly longer spin lifetime compared to the bare QD system. Finally, we have demonstrated that a relatively simple effective model yields reasonable agreement with the $\boldsymbol{k}\cdot\boldsymbol{p}$ simulation data.

[1] D. Loss and D. P. DiVincenzo, Phys. Rev. A **57**, 120 (1998).

[2] P. Recher, E. V. Sukhorukov, and D. Loss, Phys. Rev. Lett. **85**, 1962 (2000).

[3] M. Kugler, K. Korzekwa, P. Machnikowski, C. Gradl, S. Furthmeier, M. Griesbeck, M. Hirmer, D. Schuh, W. Wegscheider, T. Kuhn, C. Schüller, and T. Korn, Phys. Rev. B **84**, 085327 (2011).

[4] M. Gawełczyk and P. Machnikowski, Phys. Rev. B **87**, 195315 (2013).

[5] N. H. Bonadeo, J. Erland, D. Gammon, D. Park, D. S. Katzer, and D. G. Steel, Science **282**, 1473 (1998).

[6] T. M. Godden, J. H. Quilter, A. J. Ramsay, Y. Wu, P. Brereton, I. J. Luxmoore, J. Puebla, A. M. Fox, and M. S. Skolnick, Phys. Rev. B **85**, 155310 (2012).

[7] D. Heiss, S. Schaeck, H. Huebl, M. Bichler, G. Abstreiter, J. J. Finley, D. V. Bulaev, and D. Loss, Phys. Rev. B **76**, 241306(R) (2007).

[8] L. Huthmacher, R. Stockill, E. Clarke, M. Hugues, C. Le Gall, and M. Atatüre, Phys. Rev. B **97**, 241413(R) (2018).

[9] J. Fischer, W. A. Coish, D. V. Bulaev, and D. Loss, Phys. Rev. B **78**, 155329 (2008).

[10] D. Brunner, B. D. Gerardot, P. A. Dalgarno, G. Wuest, K. Karrai, N. G. Stoltz, P. M. Petroff, and R. J. Warburton, Science **325**, 70 (2009).

[11] M. Vidal, M. V. Durnev, L. Bouet, T. Amand, M. M. Glazov, E. L. Ivchenko, P. Zhou, G. Wang, T. Mano, T. Kuroda, X. Marie, K. Sakoda, and B. Urbaszek, Phys. Rev. B **94**, 121302(R) (2016).

[12] A. V. Khaetskii and Y. V. Nazarov, Phys. Rev. B **61**, 12639 (2000).

[13] A. V. Khaetskii and Y. V. Nazarov, Phys. Rev. B **64**, 125316 (2001).

[14] J. I. Climente, C. Segarra, and J. Planelles, New J. Phys. **15**, 093009 (2013).

[15] A. Mielnik-Pyszczorski, K. Gawarecki, M. Gawełczyk, and P. Machnikowski, Phys. Rev. B **97**, 245313 (2018).

[16] G. E. Pikus and A. N. Titkov, in *Optical Orientation*, edited by F. Meier and B. P. Zakharchenya (Elsevier, Amsterdam, 1984), pp. 73–75 and 77–131.

[17] L. M. Roth, Phys. Rev. **118**, 1534 (1960).

[18] L. M. Woods, T. L. Reinecke, and R. Kotlyar, Phys. Rev. B **69**, 125330 (2004).

[19] C. Lü, J. L. Cheng, and M. W. Wu, Phys. Rev. B **71**, 075308 (2005).

[20] D. V. Bulaev and D. Loss, Phys. Rev. Lett. **95**, 076805 (2005).

[21] H. Wei, M. Gong, G.-C. Guo, and L. He, Phys. Rev. B **85**, 045317 (2012).

[22] H. Wei, G.-C. Guo, and L. He, J. Appl. Phys. **116**, 204304 (2014).

[23] H. Wei, G.-C. Guo, and L. He, Phys. Rev. B **89**, 245305 (2014).

[24] C. Segarra, J. Planelles, J. I. Climente, and F. Rajadell, New J. Phys. **17**, 033014 (2015).

[25] K. Gawarecki and M. Krzykowski, Phys. Rev. B **99**, 125401 (2019).

[26] H. R. Trebin, U. Rössler, and R. Ranvaud, Phys. Rev. B **20**, 686 (1979).

[27] G. Bir and G. Pikus, Fiz. Tverd. Tela (Leningrad) **3**, 3050 (1961)[Sov. Phys. Solid State **3**, 2221 (1962)].

[28] R. Winkler, *Spin-Orbit Coupling Effects in Two-Dimensional Electron and Hole Systems* (Springer, Berlin, 2003).

[29] K. Suzuki and J. C. Hensel, Phys. Rev. B **9**, 4184 (1974).

[30] J. C. Slater and G. F. Koster, Phys. Rev. **94**, 1498 (1954).

[31] J.-M. Jancu, R. Scholz, F. Beltram, and F. Bassani, Phys. Rev. B **57**, 6493 (1998).

[32] M. Zieliński, Phys. Rev. B **86**, 115424 (2012).

[33] Y. Tan, M. Povolotskyi, T. Kubis, T. B. Boykin, and G. Klimeck, Phys. Rev. B **94**, 045311 (2016).

[34] G. Dresselhaus, Phys. Rev. **100**, 580 (1955).

[35] K. Roszak, V. M. Axt, T. Kuhn, and P. Machnikowski, Phys. Rev. B **76**, 195324 (2007).

[36] K. Nishi, H. Saito, S. Sugou, and J.-S. Lee, Appl. Phys. Lett. **74**, 1111 (1999).

[37] E. Goldmann, S. Barthel, M. Florian, K. Schuh, and F. Jahnke, Appl. Phys. Lett. **103**, 242102 (2013).

[38] P. Mrowiński, A. Musiał, K. Gawarecki, Ł. Dusanowski, T. Heuser, N. Srocka, D. Quandt, A. Strittmatter, S. Rodt, S. Reitzenstein, and G. Sek, Phys. Rev. B **100**, 115310 (2019).

[39] C. Pryor, J. Kim, L. W. Wang, A. J. Williamson, and A. Zunger, J. Appl. Phys. **83**, 2548 (1998).

[40] G. Bester, X. Wu, D. Vanderbilt, and A. Zunger, Phys. Rev. Lett. **96**, 187602 (2006).

[41] M. A. Caro, S. Schulz, and E. P. O'Reilly, Phys. Rev. B **91**, 075203 (2015).

[42] T. B. Bahder, Phys. Rev. B **41**, 11992 (1990).

[43] T. Andlauer, R. Morschl, and P. Vogl, Phys. Rev. B **78**, 075317 (2008).

[44] K. Gawarecki, Phys. Rev. B **97**, 235408 (2018).

[45] P. Pfeffer and W. Zawadzki, Phys. Rev. B **41**, 1561 (1990).

[46] H. Mayer and U. Rössler, Phys. Rev. B **44**, 9048 (1991).

[47] See Supplemental Material at http://link.aps.org/supplemental/10.1103/PhysRevB.102.205301 for explicit forms of all the matrices, in terms of which the eight-band $k \cdot p$ Hamiltonian terms in Sec. II are given.

[48] J.-M. Jancu, R. Scholz, E. A. de Andrada e Silva, and G. C. La Rocca, Phys. Rev. B **72**, 193201 (2005).

[49] M. Cardona, N. E. Christensen, and G. Fasol, Phys. Rev. B **38**, 1806 (1988).

[50] W. Howlett and S. Zukotynski, Phys. Rev. B **16**, 3688 (1977).

[51] D. G. Seiler, B. D. Bajaj, and A. E. Stephens, Phys. Rev. B **16**, 2822 (1977).

[52] M. I. D'yakonov, V. A. Marushchak, V. I. Perel', and A. N. Titkov, Zh. Eksp. Teor. Fiz. **90**, 1123 (1986)[Sov. Phys. JETP **63**, 655 (1986)].

[53] R. Ranvaud, H. R. Trebin, U. Rössler, and F. H. Pollak, Phys. Rev. B **20**, 701 (1979).

[54] M. Silver, W. Batty, A. Ghiti, and E. P. O'Reilly, Phys. Rev. B **46**, 6781 (1992).

[55] A. Grodecka, L. Jacak, P. Machnikowski, and K. Roszak, in *Quantum Dots: Research Developments*, edited by P. A. Ling (Nova Science, New York, 2005), pp. 47–88.

[56] M. S. M. Levinshtein and S. Rumyantsev, *Handbook Series on Semiconductor Parameters. Volume 2: Ternary and Quaternary III-V Compounds* (World Scientific, London, 1999).

[57] T. Eissfeller, Ph.D. thesis, Technical University of Munich, 2012.

[58] T. Uenoyama and L. J. Sham, Phys. Rev. B **42**, 7114 (1990).

[59] J. S. Blakemore, J. Appl. Phys. **53**, R123 (1982).

[60] S. Adachi, *Physical Properties of III-V Semiconductor Compounds* (Wiley, New York, 1992).

[61] K. Gawarecki and M. Zieliński, Phys. Rev. B **100**, 155409 (2019).

[62] http://wcss.pl